Carbon Nanotubes

DOI: 10.1002/ange.201106566

Multifunctional Ferromagnetic Carbon-Nanotube Arrays Prepared by Pulse-Injection Chemical Vapor Deposition**

Vinay Gupta and Ravinder Kumar Kotnala*

Multiwalled carbon nanotubes (MWCNTs) have received enormous attention during the past decade owing to their potential in the miniaturization of electronic[1] and mechanical[2] devices such as field-effect transistors (FET),[3] logic circuits,[4] field-emission displays,[5] energy storage systems,[6,7] optoelectronic switch and memory devices.[8] Although the idea of using MWCNTs in microelectromechanical systems (MEMS) is proposed,[9] building highly magnetic MWCNTs architectures remained a challenge in spite of their various applications in micro/nano magnetomechanical systems (MMMS/NMMS), high-flux magnetic separations, and controlled drug delivery.[10] MWCNTs can be doped with magnetic nanoparticles by chemical vapor deposition (CVD), either on various substrates, such as metals, quartz, and silicon,[6,7] or by template growth inside porous alumina.[11,12] Herein, for the first time, by pulse-injection CVD process, using ferrocene in toluene, we have grown a highly ferromagnetic three-dimensional freestanding pillar architecture of MWCNTs encapsulating iron compounds. The magnetic manipulations of mechanical motions of MWCNTs are shown and their biological compatibility, higher delivery efficiency, a prolonged release of cancer drug doxorubicin (Dox), and good targeting capabilities of Dox onto HeLa cells is demonstrated.

Figure 1a shows the optical image of freestanding Fe_3C@MWCNT array of macroscopic dimensions. The relationship between the MWCNT array thickness and growth time is shown in Figure 1b. We have grown up to 3 mm long MWCNT arrays in the reactor. However, by this process, MWCNTs of cm lengths can be grown. The freestanding MWCNT array is easily detached from the quartz surface. The cross sectional SEM images of the MWCNT array after a growth time of approximately 210 min is shown in Figure 1c. MWCNTs bundles can easily be isolated and are shown in Figure 1d. In the X-ray diffraction (XRD) pattern of MWCNT array (Figure 1e), the observed family of peaks at high angles indicate the presence of mainly iron carbide,[11] together with some iron and iron oxides (Figure S1 in the Supporting Information). The high-resolution transmission electron microscopy (HRTEM) image (Figure 1f) shows that the pillar-like MWCNTs are linked together by Fe_3C connectors. Based on the TEM images, a possible synchronous growth mechanism of the formation of such structures (Figure 1g–i). In the initial growth period (Figure 1g), MWCNTs tend to grow perpendicular to the substrate (Figure S2 in the Supporting Information). The catalyst particle (Fe_3C) moves up with the cap of the MWCNT (Figure 1h). After certain time, the flow of ferrocene/toluene mixture is stopped for a few seconds (see Experimental Section) and the growth of MWCNT is terminated. Once the flow of toluene/ferrocene solution is restarted, a new catalyst particle forms on the terminated MWCNTs and a second layer of MWCNT begins to grow on the previous MWCNT (Figure 1i). In this way, MWCNTs grow on top of each other. The Fe_3C@MWCNTs were found to be superhydrophobic and semiconducting in nature,[7] (Figure S3 and S4 in the Supporting Information). Figure 1j shows the HRTEM images of metal particle encapsulated in the graphene shells. The corresponding EDX (STEM) spectra gives agrees with Fe_3C composition (Figure 1k).

Figure 2a shows the M versus H hysteresis loop of Fe_2O_3 nanoparticles (NPs) and Fe_3C@MWCNT at room temperature (Figure S5 in the Supporting Information). The shape of hysteresis loop indicates the stronger ferromagnetic nature of Fe_3C@MWCNT as compared to Fe_2O_3 NPs. The remarkable features in the Fe_3C@MWCNT M versus H loop are coercivity (H_c) of approximately 760 Oe and remanence-to-saturation ratio (M_r/M_s) of 0.5 which are very high in comparison to other metals in MWCNT/metal nano-composites synthesized to date (Figure 2c; The values of H_C were taken directly from the given references, irrespective of being pure metal or in the form of carbon/metal composites).[12–18] The corresponding relationship between diameters of the metal NPs and H_c (Figure 2c, inset) confirms the exceptional magnetic characteristics of Fe_3C@MWCNT synthesized by the pulse-injection CVD. It is well know that for single-domain particles with a uniaxial anisotropy and randomly distributed easy axis, the ratio M_r/M_s is 0.5 only at low temperatures (ca. 100 K) and generally decreases at higher temperature as a result of depinning of the domain walls in the particle.[12] The M_r/M_s ratio for Fe_3C@MWCNT is approximately 0.5 even at room temperature which accounts for its high coercivity. The ferromagnetic nature of Fe_3C@MWCNT array can result from the presence of a high density of delocalized π electrons, as is evident from the electron paramagnetic resonance (EPR) spectrum (Figure 2b), which gives g values of 2.1365 and 2.2132 for first

[*] Dr. V. Gupta, Dr. R. K. Kotnala
National Physical Laboratory, New Delhi 110012 (India)
E-mail: drvinaygupta@netscape.net
Dr. V. Gupta
Institute of Physics, Technische Universität Ilmenau
Curie-Bau Weimarer Strasse 25, Ilmenau (Germany)

[**] We thank the director for permission to publish this work, R. Bhatia, Delhi University for cytotoxicity tests, P. Solanki for technical help, Mr. S. B. Samatha for MFM measurements. V.G. thanks Prof. P. Scharff for technical support and Humboldt foundation for a Humboldt fellowship.

Supporting information for this article is available on the WWW under http://dx.doi.org/10.1002/anie.201106566.

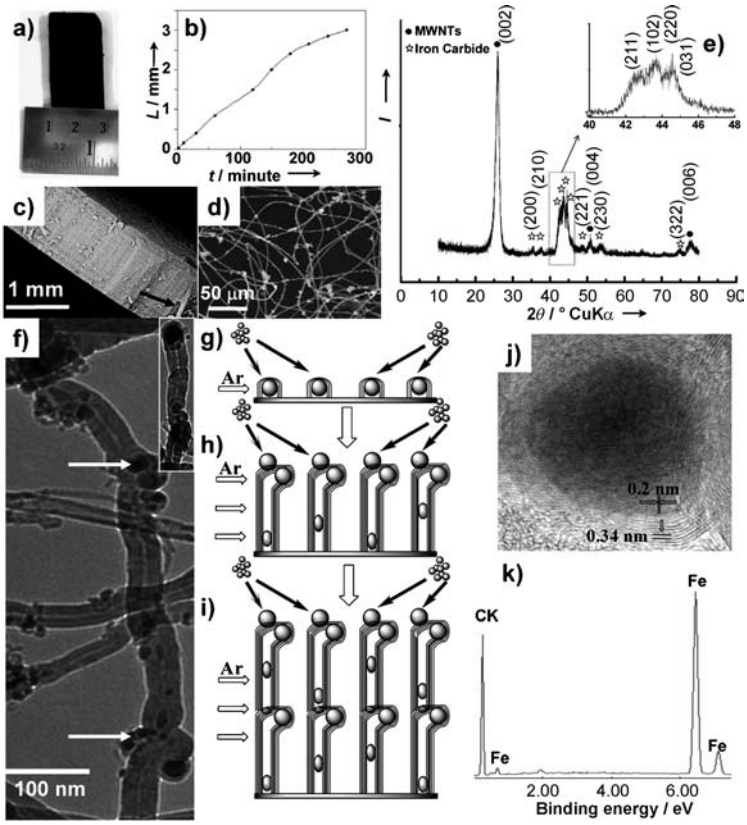

Figure 1. a) Optical image of freestanding Fe_3C@MWCNT array. b) Relationship between the nanotube film thickness *L* and the growth time. c) Cross section SEM image of the Fe_3C@MWCNT array with growth time of approximately 210 min (black arrow indicates a protruding bundle of Fe_3C@MWCNT. d) SEM image of strands of Fe_3C@MWCNT. e) XRD spectra of the Fe_3C@MWCNT array. f) HRTEM image of Fe_3C@MWCNT, showing the pillars of MWCNTs stacked on top of each linked together by Fe_3C units (indicated by the white arrows). g–i) formation mechanism of the pillars of Fe_3C@MWCNT (gray balls are Fe_3C, the middle balls in the parts (h) and (i) are indication of the direction of Fe_3C before reaching at the top). j) HRTEM of an encapsulated Fe_3C particle. k) EDX (STEM) spectra of Fe_3C encapsulated in the MWCNT.

and second peak. The second peak is quite close to the EPR curve obtained for iron carbide whereas the first peak can be due to the inter-tubular interaction or the interaction between Fe_3C and MWCNT. The *g* values are much larger than the *g* value of 2.0024 for pure carbon and are observed for highly ferromagnetic materials. The magnetic domain structure of Fe_3C@MWCNT array was further probed by magnetic force microscopy (MFM). Figure 2d shows the MFM image of the top surface of the Fe_3C@MWCNT array (see inset of Figure 2d). The MFM image reveals uniform distribution and highly aligned magnetic domains present in Fe_3C@MWCNT array. The surface roughness of the array is approximately 35 nm. The observed magnetic domains seem to be larger than the average size of Fe_3C (ca. 10 nm), this indicates that a long-range magnetic interactions exist in the Fe_3C@MWCNT array. The magnetic field of the catalyst particles is extended beyond its domain boundaries. Extended single magnetic domains of catalyst can be also be observed in the magnetic phase contours recorded using off-axis electron holography of a single catalyst filled MWCNT.[12] It is possible to align electrons present in MWCNT by two magnetic forces, that is, one is due to the applied magnetic field and the other is induced by the magnetization of the Fe_3C present in MWCNT. The delocalized electrons in a MWCNT, sandwiched between the two fields, can be induced to align along the same direction as the magnetic field of the Fe_3C and may contribute to the ferromagnetism. This situation is evident from the high spin concentration of 2.777×10^{20} spins g^{-1} for the Fe_3C@MWCNT array (calculated from EPR), which is four-orders of magnitude higher than for pure carbon. Therefore the alignment of a significant number of delocalized π electrons of both Fe_3C and MWCNT can take place in a highly coercive way.

Some of the possible modes of an Fe_3C@MWCNT actuator, and a diagram of Fe_3C@MWCNT as a magnetic paddle are shown in Figures 3a and b, respectively. Magnetic force by an external magnetic stirrer can induce mechanical motion in Fe_3C@MWCNT (Figure 3c) films on the surface of water. The rotation of the Fe_3C@MWCNT array is shown in the bottom inset of Figure 3c (See Movie S1 in the Supporting Information). It is possible to rotate the Fe_3C@MWCNT array at the speed of magnetic stirrer for many ten thousand of cycles without any degradation in the performance. The top inset of Figure 3c shows an ideal nanomagnetic paddle composed of a single MWCNT that can be used as a rotary nanomagnetic paddle for nanofluidics.

Targeted drug delivery systems (TDDS) deliver drug to the targeted organ or cell without affecting other sites. However, many drugs are water insoluble. Therefore, drugs need a carrier that is water soluble as well as biocompatible. We have functionalized Fe_3C@MWCNT with methylene blue (MB; Supporting Information, Figure S6 and S7), which is itself a very effective drug for detecting and curing several diseases.[19–21] Figure 4a shows schematically the of salmon testes DNA to MB-Fe_3C@MWCNT. Photoluminescence (PL) spectroscopy is very sensitive to the surface characteristics. Figure 4b shows the PL characteristics of Fe_3C@MWCNT, MB, and DNA and confirm successful binding of Fe_3C@MWCNT with MB and DNA.

The loading and release performance of Fe_3C@MWCNT is compared with a clinically used magnetic carrier, Fe_3O_4 NPs (Figure 4d and e). Figure 4d shows the absorption isotherm of the cancer drug doxorubicin (Dox) on Fe_3C@MWCNT as well as Fe_3O_4 NPs, with the maximum loading capacity of approximately 43 and 28 μg mg^{-1}, respectively, where the MWCNT surface provides sufficient surface area for π–π stacking interaction for drug absorption. The in vitro release of Dox from Fe_3C@MWCNT and Fe_3O_4 NPs was examined by dialyzing Dox/NPs composites in PBS buffer solutions. The Fe_3O_4 NPs (Figure 4e) shows a burst release of Dox with more than 95% release in one day, which can be disadvantageous to drug efficiency, if a slow release is desired. On the other hand, the release of Dox from Fe_3C@MWCNT is

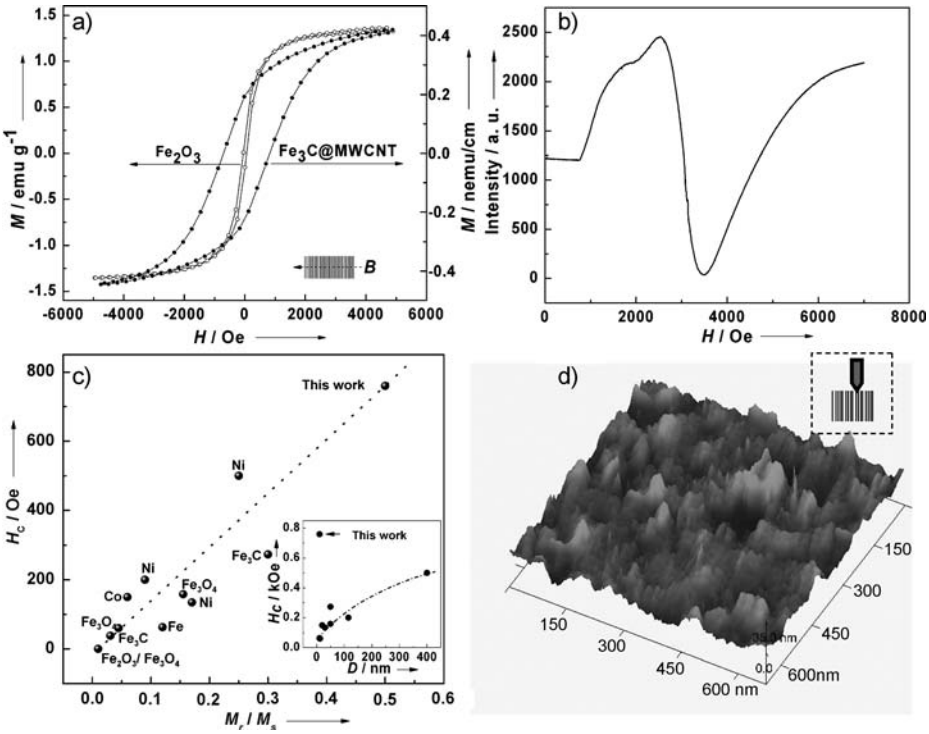

Figure 2. a) *M* versus *H* curves for Fe_2O_3 nanoparticles and Fe_3C@MWCNT (*B* indicates magnetic field, lines the nanotubes, and arrow the direction of the magnetic field). b) EPR spectrum of Fe_3C@MWCNT. c) Relationship between coercitivity and remanent/saturation magnetization for various metals. Inset: relationship between coercitivity and NP diameter (at 300 K). d) Magnetic force microscope image of the Fe_3C@MWCNT array at 25 °C (the inset shows that the scanning was performed perpendicular to the tube axis).

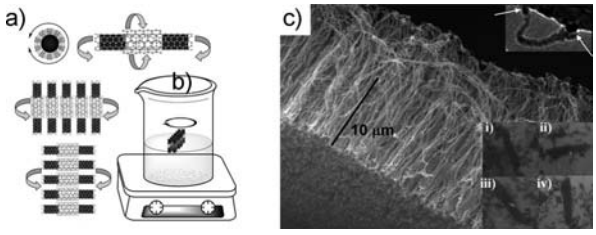

Figure 3. a) Schematic illustrations of different modes of rotation of the Fe_3C@MWCNT array in the presence of a magnetic field. b) Set up for Fe_3C@MWCNT array in a liquid and rotated with the help of a magnetic stirrer plate. c) The thickness of the Fe_3C@MWCNT array used for rotation, lower inset (i–iv) shows the sequence of rotation of a 4 mm long and 15 μm thick Fe_3C@MWCNT array (Video V1 in the Supporting Information). The top inset shows the single-Fe_3C@MWCNT stirrer bar capped with Fe_3C at both ends (indicated by the white arrows).

comparatively slow with only 38% release in one day. This suggests that Fe_3C@MWCNT is more effective than Fe_3O_4 for drug delivery if a slow drug release is required.

The biocompatibility of Fe_3C@MWCNT was evaluated using the MTT cytotoxicity assays in which the HeLa cells were seeded in 96-well plate (Figure 4c). Figure 4f shows the viability of HeLa cells to Fe_3C@MWCNT with or without Dox. As the concentration of Fe_3C@MWCNT increases so does the effectiveness of Dox. The results show promising targeting capabilities and biocompatibility of Fe_3C@MWCNT.

As shown in the circular dichroism (CD) spectra of DNA (Figure 4g) treated with MB-Fe_3C@MWCNT in different ratios, as the concentration of MB-Fe_3C@MWCNT is increased, there was decrease in the ellipticity of the DNA without change in peak positions, which indicates that interaction with MB-Fe_3C@MWCNT causes some instability in DNA, but it does not change its conformation even at high MB-Fe_3C@MWCNT concentration. This indicates that MB-Fe_3C@MWCNTs interact with DNA but do not cause any major breaks or unfolding of it and are thus DNA compatible. (Figure S8 in the Supporting Information for the compatibility of Fe_3C@MWCNTs with BSA protein). Moreover, the limitations that essentially the internal MWCNT space is not available for drug attachment due to the presence of Fe_3C particles, means that any substance attachment can take place only on the external surface, thus reducing the total gravimetric loading capacity and help prevent burst release of drug.

Experimental Section

A ferrocene [bis(cyclopentadienyl)iron(II)]/toluene system was used for the growth of vertically aligned Fe_3C@MWCNT onto quartz tubes using a pulse injection technique. A solution of 5% ferrocene in toluene was injected at the rate of 0.2 mL min^{-1} with a syringe pump into a quartz reactor's first zone maintained at 350 °C, which was carried to the second zone maintained at 800 °C with the help of continuous Ar flow. The flow was stopped for a few seconds after every minute. This process was carried out from few minutes to a few hours.

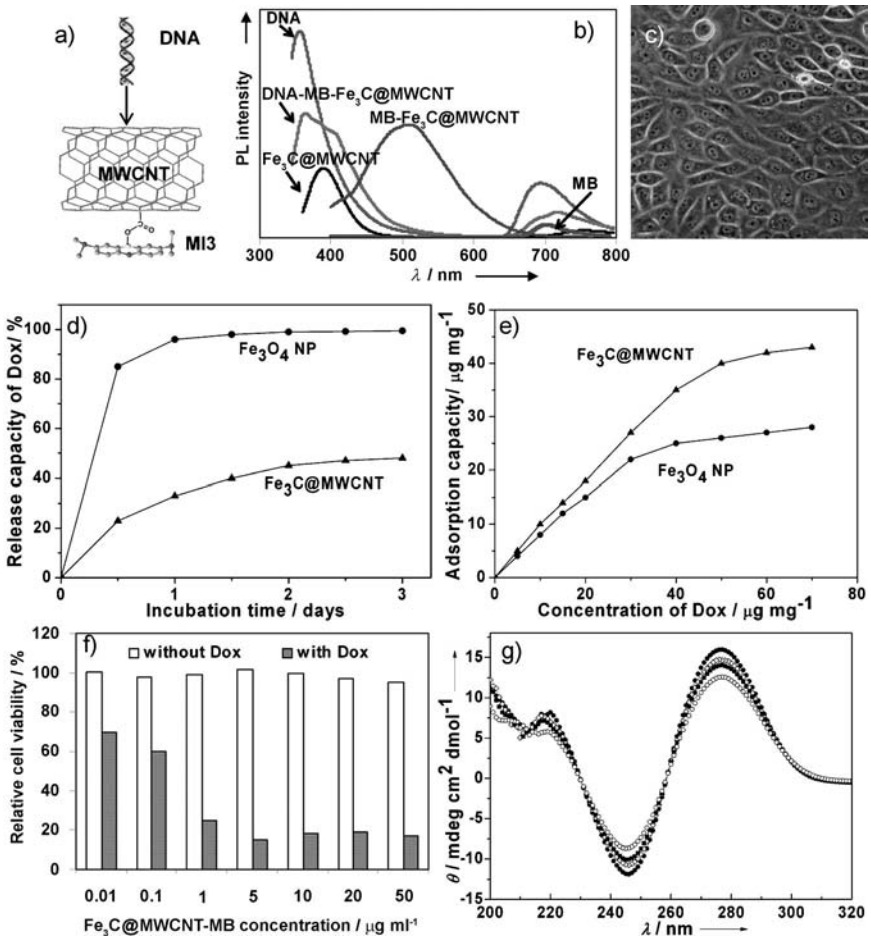

Figure 4. a) Schematic of the DNA attachment to MB-Fe_3C@MWCNT. b) PL spectra. c) Optical image of HeLa cell line treated with Fe_3C@MWCNT. d) In vitro Dox adsorption isotherm. e) Release isotherm of Dox. f) Viability of HeLa cells treated with Fe_3C@MWCNT in the presence and absence of Dox. g) CD spectra of DNA treated with different concentrations (filled circle: control DNA, diamond: 1:1 DNA/MWCNT, filled square: 1:3 DNA/MWCNT, open circle: 1:5 DNA/MWCNT) of MB-Fe_3C@MWCNT.

The MWCNTs were characterized by XRD, SEM, EDX, TG/DTA, TEM, VSM, MFM, CD, MTT assay (see Supporting Information for details).

Received: September 15, 2011
Published online: February 8, 2012

Keywords: carbon nanotubes · chemical vapor deposition · DNA · drug release · magnetic properties

[1] P. Avouris, Z. H. Chen, V. Perbeinos, *Nat. Nanotechnol.* **2007**, *2*, 605 – 615.
[2] J. W. Judy, *Smart Mater. Struct.* **2001**, *10*, 1115 – 1134.
[3] A. Javey, J. Guo, Q. Wang, M. Lundstrom, H. Dai, *Nature* **2003**, *424*, 654 – 656.
[4] Z. Chen, *Science* **2006**, *311*, 1735.
[5] L. Gangloff, E. Minoux, K. B. K. Teo, P. Vincent, V. T. Semet, V. T. Binh, M. H. Yang, I. Y. Y. Bu, R. G. Lacerda, G. Pirio, J. P. Schnell, D. Pribat, D. G. Hasko, G. A. J. Amaratunga, W. I. Milne, P. Legagneux, *Nano Lett.* **2004**, *4*, 1575 – 1579.
[6] S. Talapatra, S. Kar, S. K. Pal, R. Vajtai, L. Ci, P. Victor, M. M. Shaijumon, S. Kaur, O. Nalamasu, P. M. Ajayan, *Nat. Nanotechnol.* **2006**, *1*, 112 – 116.
[7] L. Ci, S. M. Manikoth, X. Li, R. Vajtai, P. M. Ajayan, *Adv. Mater.* **2007**, *19*, 3300 – 3303.
[8] J. Borghetti, V. Derycke, S. Lenfant, P. Chenevier, A. Filoramo, M. Goffman, D. Vuillaume, J. P. Bourgoin, *Adv. Mater.* **2006**, *18*, 2535 – 2540.
[9] A. M. Fennimore, T. D. Yuzvinsky, W.-Q. Han, M. S. Fuhrer, J. Cumings, *Nature* **2003**, *424*, 408 – 410.
[10] H. Terrones, F. López-Urías, E. Muñoz-Sandoval, J. A. Rodríguez-Manzo, A. Zamudio, A. L. Elías, M. Terrones, *Solid State Sci.* **2006**, *8*, 303 – 320.
[11] E. C. Vermisoglou, G. N. Karanikolos, G. Pilatos, E. Devlin, G. E. Romanos, C. M. Veziri, N. K. Kanellopoulos, *Adv. Mater.* **2010**, *22*, 473 – 477.
[12] D. Mattia, G. Korneva, A. Sabur, G. Friedman, Y. Gogotsi, *Nanotechnology* **2007**, *18*, 155305.
[13] M. A. Correa-Duarte, M. Grzelczak, V. Salgueiriño-Maceira, M. Giersig, L. M. Liz-Marzán, M. Farle, K. Sierazdki, R. Diaz, *J. Phys. Chem. B* **2005**, *109*, 19060.
[14] E. C. Vermisoglou, G. Pilatos, G. E. Romanos, E. Devlin, N. K. Kanellopoulos, G. N. Karanikolos, *Nanotechnology* **2011**, *22*, 355602.
[15] M. D. Baró, B. J. Nelson, *Nanotechnology* **2011**, *22*, 275713.
[16] H. J. Song, N. Li, X. Jing, X. Yang, H. Tang, *J. Nanopart. Res.* **2011**, *13*, 5457 – 5464.
[17] J. P. Cheng, X. B. Zhang, G. F. Yi, Y. Ye, M. S. Xia, *J. Alloys Compd.* **2008**, *455*, 5 – 9.
[18] K. Koziol, T. Kasama, R. E. Dunin-Borkowski, P. Barpanda, A. H. Windle, *Proc. Mater. Res. Soc. Symp. USA* **2006**, *962E*, P13.03.
[19] C. R. Martin, P. Kohli, *Nat. Rev. Drug Discovery* **2003**, *2*, 29 – 37.
[20] H. Atamna, A. Nguyen, C. Schultz, K. Boyal, J. Newberry, H. Kato, B. N. Ames, *FASEB J.* **2008**, *22*, 703 – 712.
[21] D. Pantarotto, R. Singh, D. McCarthy, M. Erhardt, J. P. Briand, M. Prato, K. Kostarelos, A. Bianco, *Angew. Chem.* **2004**, *116*, 5354 – 5358; *Angew. Chem. Int. Ed.* **2004**, *43*, 5242 – 5246.

